A Bidirectional Isolated DC–DC Converter as a Core Circuit of the Next-Generation Medium-Voltage Power Conversion System

Shigenori Inoue, *Student Member, IEEE*, and Hirofumi Akagi, *Fellow, IEEE*

***Abstract*—This paper describes a bidirectional isolated dc–dc converter considered as a core circuit of 3.3-kV/6.6-kV high-power-density power conversion systems in the next generation. The dc–dc converter is intended to use power switching devices based on silicon carbide (SiC) and/or gallium nitride, which will be available on the market in the near future. A 350-V, 10-kW and 20 kHz dc–dc converter is designed, constructed and tested. It consists of two single-phase full-bridge converters with the latest trench-gate insulated gate bipolar transistors and a 20-kHz transformer with a nano-crystalline soft-magnetic material core and litz wires. The transformer plays an essential role in achieving galvanic isolation between the two full-bridge converters. The overall efficiency from the dc-input to dc-output terminals is accurately measured to be as high as 97%, excluding gate drive and control circuit losses from the whole loss. Moreover, loss analysis is carried out to estimate effectiveness in using SiC-based power switching devices. Loss analysis clarifies that the use of SiC-based power devices may bring a significant reduction in conducting and switching losses to the dc–dc converter. As a result, the overall efficiency may reach 99% or higher.**

***Index Terms*—Bidirectional isolated dc–dc converter, medium-voltage power conversion systems, power density, wide-band-gap semiconductors.**

I. Introduction

WIDE-BAND-GAP semiconductors such as silicon carbide (SiC) and gallium nitride (GaN) have superior characteristics to silicon (Si). Many universities and/or manufacturers are now cooperating and competing to develop the next-generation, ultra low-loss, high-speed power devices using wide-band-gap semiconductors [1]–[9]. Infineon Technologies and Cree have already put 300-V, 600-V, and 1,200-V SiC–schottky barrier diodes (SBDs) on the market. These SiC–SBDs have been tested in power electroinic circuits to evaluate their effectiveness in reducing power loss [12]. In addition, SiC–junction field-effect transistors (JFETs) and SiC–MOSFETs are now shifting from laboratory levels toward commercial levels. Mitsubishi Electric and Rohm in December 2004, and the National Institute of Advanced Industrial Science and Technology of Japan (AIST) in March 2005, independently announced that they had developed SiC–MOSFETs with reduced channel resistances [8], [9].

Manuscript received December 1, 2005; revised May 23, 2006. Recommended for publication by Associate Editor J. R. Enslin.

The authors are with the Department of Electrical and Electronic Engineering, Tokyo Institute of Technology, Tokyo 152-8552, Japan (e-mail: inoue@akg.ee.titech.ac.jp; akagi@ee.titech.ac.jp).

Digital Object Identifier 10.1109/TPEL.2006.889939

Since SiC power devices with low conducting and switching losses can operate at higher temperature than Si counterparts can, smaller cooling devices such as heatsinks and fans are applicable. This makes a significant contribution to increasing the power density of power conversion systems.

State-of-the-art medium-voltage power conversion systems, however, usually require line-frequency (50 or 60 Hz) transformers to ensure galvanic isolation between the utility and the load. The size and weight of the transformer occupies a large part in the whole power conversion system. In other words, even if medium-voltage power conversion systems replaced Si power devices with SiC power devices, the transformer would impose limitations on the power density.

This paper describes a bidirectional isolated dc–dc converter [10], [11] considered as a core circuit of 3.3-kV/6.6-kV high-power-density power conversion systems in the next generation. Although the dc–dc converter has already been known as a technique to reduce the transformer size, few papers have dealt with this topology for many years. However, providing loss evaluation of the dc–dc converter in this paper may spur interest in this topology because new power devices and magnetic materials have been emerging. In this paper, the 350-V, 10-kW, 20-kHz dc–dc converter using latest trench-gate Si-insulated gate bipolar transistors (IGBTs) and soft magnetic material is designed, constructed, and tested as the core circuit of 3.3-kV, 270-kW adjustable-speed motor drives with regenerating braking. The tested circuit is unique in that the dc output terminals are connected back to the dc input terminals, so as to regenerate the dc output power to the dc voltage source. This special connection is useful to accurately measure the overall loss produced by the dc–dc converter. The overall efficiency from the dc-input to dc-output terminals in the experimental circuit is 96.8% at the rated power of 10 kW, and the maximum efficiency is 97.4% at 5.5 kW. Loss analysis carried out in this paper encourages to introduce SiC power devices to the dc–dc converter in terms of having the possibility of significantly reduced loss. As a result, the use of SiC-MOSFETs will improve the efficiency to 99% or higher.

II. Technical Issues in Medium-Voltage Power Conversions Systems

A. The 6.6-kV BTB (Back-to-Back) Systems

The proliferation of distributed generation based on renewable energy and fuel cells in the near future encourages the Central Research Institute of Electric Power Industry of Japan

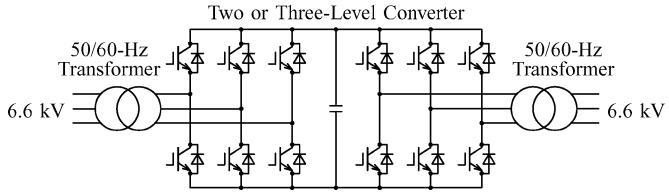

Fig. 1. Present BTB system for the 6.6-kV power distribution system.

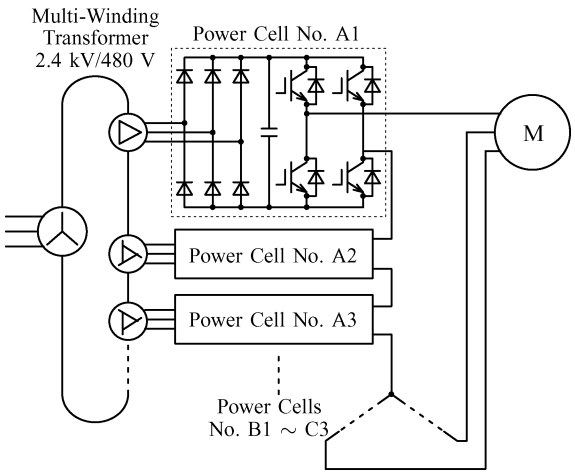

Fig. 2. Medium-voltage motor drive system proposed in [14].

in feasibility study of a 6.6-kV, 1-MW BTB system referred to as a loop power flow controller [13]. Fig. 1 shows the circuit configuration of the 6.6-kV BTB system that will be installed between two radial distribution feeders connected to the same primary distribution transformer. The BTB system forming a single looped distribution feeder actively controls active power as well as reactive power, so as to keep each voltage referred to 100 V in a range of 95 to 107 V throughout the looped feeder. The BTB system consists of two line-frequency transformers and two voltage-source PWM converters with a common dc-link capacitor. The transformers play an important role in preventing a zero-sequence current from circulating along the looped feeder. Unfortunately, each transformer rated at 6.6 kV and 1 MVA weighs around 4,000 kg, while each BTB converter ranges from 1,000 to 2,000 kg.

The use of leading-edge power devices such as IGCTs and IEGTs or IGBTs makes it possible to eliminate the two transformers from the 6.6-kV BTB system. However, the transformerless BTB system may cause a zero-sequence current circulating along the looped feeder. In the worst case, the zero-sequence current results in inappropriate operation of line-to-ground fault protection relays. To avoid the error accompanied by line-to-ground fault detection, the circulating zero-sequence current should be reduced to less than 0.2 A in rms because the Japanese 6.6-kV utility power distribution system is a three-phase three-wire ungrounded circuit.

B. Medium-Voltage Motor Drive Systems

Fig. 2 shows a medium-voltage adjustable-speed motor drive system developed by Robicon Corp [14]. A three-phase diode

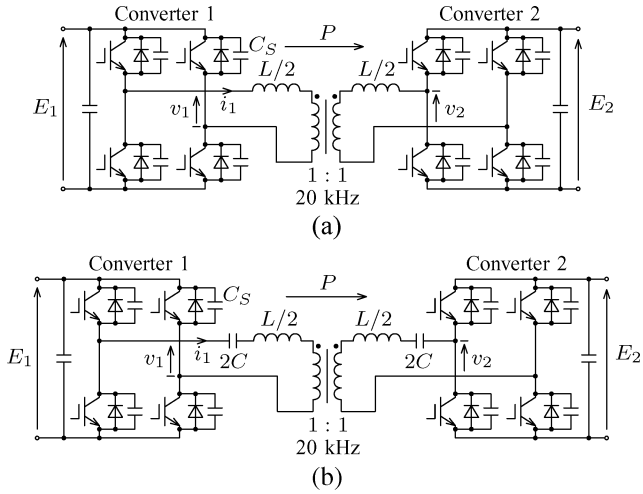

Fig. 3. Bidirectional isolated dc–dc converter: (a) based on a non-resonant circuit and (b) based on a series-resonant circuit.

rectifier and a single-phase H-bridge inverter form a power cell. The multi-winding line-frequency transformer supplies three-phase isolated voltages to the power cells. The ac output terminals of the power cells in each phase are connected in series to produce a sufficient voltage to drive the medium-voltage ac motor. The number of levels of the motor line-to-neutral voltage depends on how many cells are cascaded per phase. Moreover, a special multiwinding structure reduces harmonic currents flowing into the utility grid.

Although this unique system gains wide acceptance today in the field of industrial motor drives, the weight and volume of the transformer occupies a large part in the system, and it is impossible to regenerate power back to the utility grid when the motor is decelerated.

III. Next-Generation Medium-Voltage Power Conversion Systems

This section deals with a medium-voltage power conversion system in the next generation, which is characterized by using bidirectional isolated dc–dc converters as the core circuit. This makes it possible to eliminate a line-frequency transformer from medium-voltage power conversion systems.

A. Bidirectional Isolated DC–DC Converter

The bidirectional isolated dc–dc converters shown in Fig. 3 can galvanically isolate the output terminals from the input terminals, and can step up and down its output voltage by using a high-frequency transformer [10], [11].

Fig. 3 shows two possible circuits of a bidirectional isolated dc–dc converter. Fig. 3(a) is based on a non-resonant circuit while (b) is on a resonant circuit. In Fig. 3(b), the voltage across the transformer terminals becomes nearly sinusoidal by adjusting the operating frequency to the resonant frequency $(= 1/2\pi\sqrt{LC})$ so that the power devices can operate in zero-current switching (ZCS) manner.

This paper deals with 3.3-kV or 6.6-kV power conversion systems based on the bidirectional isolated dc–dc converter. In this case, the dc-link voltage in the dc–dc converter is less than

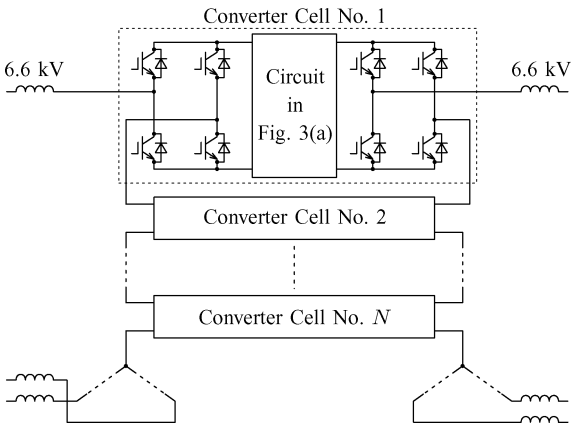

Fig. 4. 6.6-kV BTB system in the next generation.

1 kV. The weight and volume of the resonant capacitors C in Fig. 3(b) is not negligible. Hence, it is more practical to employ the non-resonant dc–dc converter in Fig. 3(a), and so this paper focuses only on Fig. 3(a).

When [10] and [11] were published, the dc–dc converters did not draw much attention as a core circuit of medium-voltage power conversion systems because the first-generation IGBTs at that time suffered from non-negligible conducting and switching losses (see Table IV). Fortunately, the advances of power device technology and magnetic material make the dc–dc converter feasible for elimination of bulky and heavy line-frequency transformers from power conversion systems.

Pavlovsky *et al.* have designed, constructed and experimentally verified a bidirectional isolated dc–dc converter rated at 750 V/600 V, 50 kW, and 25 kHz with a resonant ZVS and quasi-ZCS switching scheme that is different from the dc–dc converter in this paper [15]. The efficiency of their dc–dc converter was estimated to be as high as 97%, using trench-gate Si-IGBTs together with a transformer consisting of an amorphous core and foil windings. However, neither loss analysis was carried out, nor medium-voltage application was considered in [15].

B. Next-Generation 6.6-kV BTB System

Fig. 4 depicts the 6.6-kV back-to-back (BTB) system in the next-generation. Each converter cell consists of a bidirectional isolated dc–dc converter and two single-phase PWM converters connected to the input and output terminals of the dc–dc converter. Cascade connection of N converter cells forms the BTB system.

Table I summarizes design examples of the converter cells. The dc-link voltage of a converter cell depends on N, the number of cascade connection. If N is designed to be nine, the ac-side rms voltage of a single converter cell is $6{,}600/9\sqrt{3} = 423$ V, and the dc-link voltage is 677 V, allowing to use 1.2-kV IGBTs. In this case, the nine cascaded converter cells in each phase produce nineteen-level voltage waveform at the ac side in each phase. Thus, switching ripples can be suppressed by only the ac-link inductors without any switching ripple filter. Since the switching frequency of the PWM converters is 1 kHz, their switching losses can be negligible.

TABLE I
DESIGN EXAMPLES OF THE CONVERTER CELL USED FOR THE NEXT-GENERATION BTB SYSTEM FOR THE 6.6-kV POWER DISTRIBUTION SYSTEM

N	Waveform	AC Input	DC Link	Device Rating
4	9 Level	952 V	1.52 kV	2.4 kV
5	11 Level	752 V	1.22 kV	2.0 kV
6	13 Level	635 V	1.02 kV	1.7 kV
7	15 Level	544 V	870 V	1.7 kV
8	17 Level	476 V	762 V	1.4 kV
9	19 Level	423 V	677 V	1.2 kV

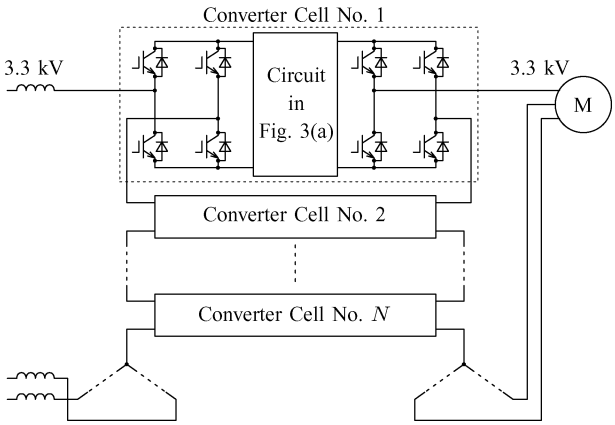

Fig. 5. 3.3-kV motor drive in the next generation.

C. Medium-Voltage Motor Drive System in the Next Generation

Fig. 5 shows the 3.3-kV motor drive system in the next generation. The converter cells are cascaded and a 3.3-kV ac motor is connected to the ac output terminals. The system requires cascaded PWM converters at the line side because diode rectifiers instead of the PWM converters produce a large amount of harmonic current. Moreover, the PWM converters play an important role in balancing the dc-link voltages as well as providing regenerative braking capability.

If the rated power of the motor drive system is 270 kW with $N = 9$, the rated power of a single converter cell is 10 kW, and the dc-link voltage becomes 339 V, allowing to use 600-V IGBTs. Thus, this paper designs, constructs, and tests a bidirectional isolated dc–dc converter rated at 350 V, 10 kW, and 20 kHz, and analyzes the losses to estimate effectiveness in the use of SiC power devices.

In Germany, Austria, and Switzerland, the electrical railways are fed by single-phase 15-kV, 16 2/3-Hz power lines. This results in bulky and heavy low-frequency transformers on locomotives. Many reaserchers/engineeres in Europe have been tackling this issue and have proposed several different solutions to date [16]. Among them, the traction systems in [17] and [18] are similar to the system in Fig. 5, although they are different in application, voltage levels, and the use of the resonant dc–dc converter shown in Fig. 3(b). However, few experimental results have been reported yet about the traction system. Heinemann has designed, constructed and tested a prototype of a 3-kV,

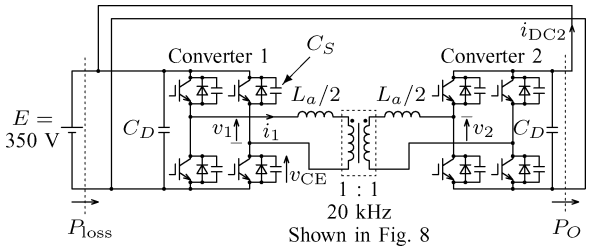

Fig. 6. Experimental circuit configuration for achieving precisely measuring the overall loss and loss analysis.

TABLE II
CIRCUIT PARAMETERS IN FIG. 6

DC power supply voltage	E	350 V
Rated power	P	10 kW
DC capacitor	C_D	2,000 μF
Snubber capacitor	C_S	0.01 μF (1.5%)
Inductor	$L_a/2$	10.5 μH (11%)
Inductor resistance	$R_a/2$	4.5 mΩ (0.037%)
Transformer core material		FT-3M
Transformer turn number		17 : 17
Transformer leakage inductance	$L_{\rm trans}$	1.6 μH (1.6%)
Transformer winding resistance	$R_{\rm trans}$	17 mΩ (0.14%)

On a single-phase 350-V, 10-kW, 20-kHz base.

350-kVA, 10-kHz transformer having an insulation capability of 35 kV [19], which has been intended to be used in the traction system in [18].

IV. Design and Characteristics of the DC–DC Converter as the Core Circuit

A. Circuit Configuration

Fig. 6 shows the circuit configuration of the 350-V, 10-kW, 20-kHz bidirectional isolated dc–dc converter for experiments. Table II summarizes the circuit parameters in Fig. 6. Fig. 8 shows the photograph of the transformer rated at 350 V, 10 kVA, and 20-kHz. Two full-bridge voltage-source converters (Converters 1 and 2) are connected symmetrically via the transformer. The output power P_O is regenerated back to the input terminals so that the overall loss of the circuit $P_{\rm loss}$ can be measured accurately and easily as the output power of the dc voltage source E. In the experiment, a digital power meter (Yokogawa WT130) is used to measure the overall loss $P_{\rm loss}$. An analog ammeter (Yokogawa 2011 37) measures the average dc output current $I_{\rm DC2}$ so that the output power P_O can be obtained as $E \cdot I_{\rm DC2}$.

The latest trench-gate IGBTs (Mitsubishi Electric CM200DY-12NF) are used in Converters 1 and 2. The core material of the transformer is "Finemet" FT-3M manufactured by Hitachi Metals. A set of litz wires is used as the windings to reduce the influence by the so-called skin effect. Two identical auxiliary inductors consisting of ferrite cores and litz wires are connected to adjust the inductance value that affect the power flow to be $L = L_{\rm trans} + L_a = 22.6$ μH. The winding resistance of the transformer and the inductors are $R = R_{\rm trans} + R_a = 26$ mΩ[1]

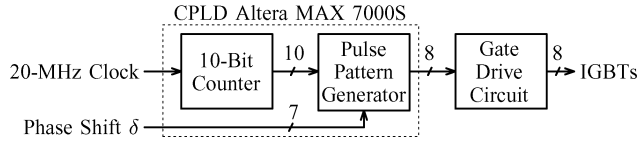

Fig. 7. Control circuit of the dc–dc converter.

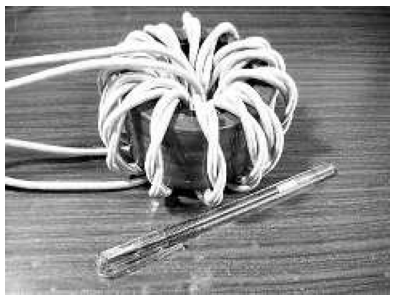

Fig. 8. 350-V, 10-kVA, and 20-kHz transformer.

If all the power devices, the transformer, and the auxiliary inductors were ideal, the ac-side voltage of Converters 1 and 2, v_1 and v_2, would be rectangular voltage at $f = 20$ kHz. The output power P_O is determined by the phase shift δ [rad] between v_1 and v_2 as follows [10]:

$$P = \frac{E^2}{\omega L}\left(\delta - \frac{\delta^2}{\pi}\right) \tag{1}$$

where $\omega = 2\pi f$.

Connecting a snubber capacitor C_S in parallel to each IGBT in Fig. 6 realizes zero-voltage switching (ZVS) operation. The minimum required current $I_{\rm min}$ flowing in an IGBT to ensure ZVS operation is determined by [11]:

$$I_{\rm min} = \frac{2E}{\sqrt{L/C_S}}. \tag{2}$$

B. Control Circuit

Fig. 7 depicts the block diagram of the control and gate drive circuit. A clock signal at 20 MHz is fed to the CPLD (complex programmable logic device) Altera MAX 7000S (EPM7160SLC84-10). The 10-b counter counts the clock pulse to create 10-b digital sawtooth signal at 20 kHz. The pulse pattern generator receives the digital sawtooth signal and the 7-b phase shift δ to generate switching patterns. A dead time of 500 ns is also created in the pulse pattern generator. The least significant bit (LSB) in the 7-b phase shift δ corresponds to 0.36° (2π/1,000 [rad]) because the clock period of 50 ns (20 MHz) is 0.1% of the switching period of 50 μs (20 kHz) in the dc–dc converter. The gate drive circuit finally produces proper gate-emitter voltages (+15 V to be turned on and −15 V to be turned off) for the eight IGBTs.

Note that the control circuit in this paper is an open-loop system. Feedback control, for example, to control the power

[1]These inductance and resistance values ($L_{\rm trans}$, L_a, $R_{\rm trans}$, and R_a) were at 10 kHz and separately obtained by using an LCR meter (Agilent Technologies 4263B).

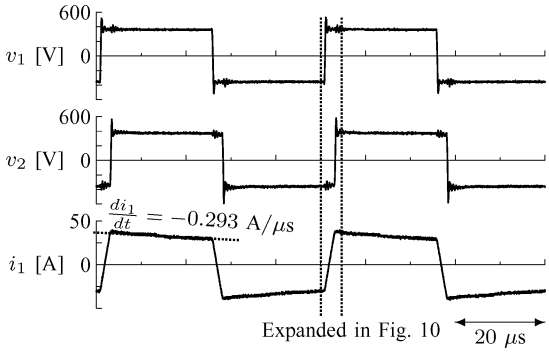

Fig. 9. Experimental waveforms when a power of 10 kW is delivered.

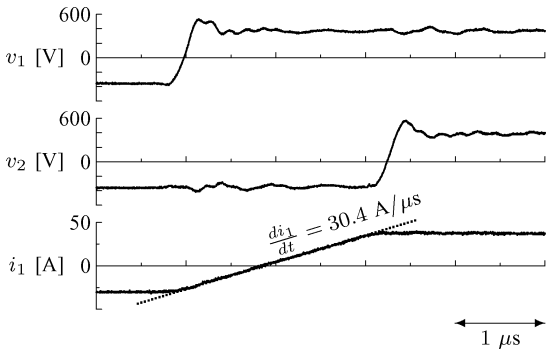

Fig. 10. Time-expanded waveforms of Fig. 9.

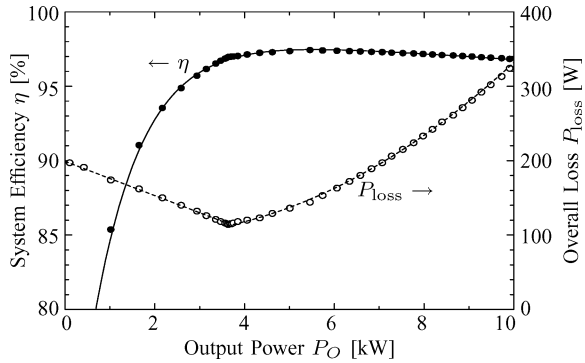

Fig. 11. Relationships between the output power P_O, the system efficiency η and the overall loss $P_{\rm loss}$.

or the dc-link voltage constant, can be easily realized when installing analog-to-digital converters.

C. Conversion Efficiency and Overall Loss

Fig. 9 shows experimental waveforms at the rated power of $P_O = 10$ kW. Fig. 10 shows the time-expanded waveforms of Fig. 9. In this case, the phase shift δ was 17°, the rms value of the current i_1, I_1, was 32.6 A, and the average value of the absolute value of i_1, $\langle |i_1| \rangle$, was 32.0 A.

The overall loss in the circuit $P_{\rm loss}$ was 335 W. Hence, the system efficiency η from dc input to dc output was $P_O/(P_O + P_{\rm loss}) = 96.8\%$.[2] The di_1/dt values in Figs. 9 and 10 are used in the following loss analysis procedure.

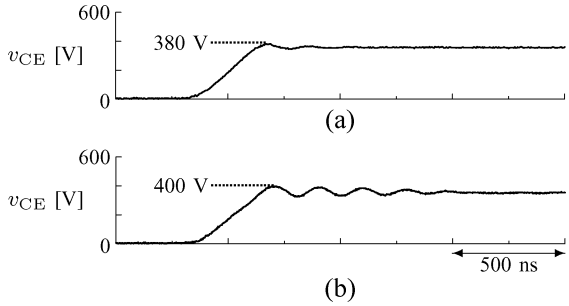

Fig. 12. Waveforms of the collector-emitter voltage of the IGBT: (a) when $P_O = 0$ kW and (b) when $P_O = 10$ kW.

Fig. 11 describes the relationships between the output power P_O, the system efficiency η, and the overall loss $P_{\rm loss}$. The overall loss $P_{\rm loss}$ reaches its minimum at around $P_O = 3.8$ kW. When P_O is below 3.8 kW, incomplete ZVS operation results in forming a short circuit of the snubber capacitors that store some amount of energy so that the switching loss takes dominance. On the other hand, when P_O exceeds 3.8 kW, the conducting loss of the IGBTs becomes dominant. At $P_O = 5.5$ kW, the system efficiency η reaches its maximum, 97.4%.

D. Overvoltage Across the IGBTs

Fig. 12 is the collector-emitter voltage across an IGBT in Converter 1, $v_{\rm CE}$, when the IGBT is turned off. Note that $v_{\rm CE}$ is not the voltage on the IGBT chip but the voltage across the collector and emitter terminals of the IGBT module. Fig. 12(a) was observed when the output power P_O was zero, and (b) was observed when P_O was 10 kW. Closely connecting the snubber capacitors C_S between the IGBT collectors and emitters and careful optimization of the gate resistance in the gate-drive circuit suppressed the maximum overvoltage to be 380 V when $P_O = 0$ kW and 400 V $P_O = 10$ kW at $E = 350$ V.

E. Loss at $P_O = 0$ kW

When the output power P_O is zero, all the energy stored in a snubber capacitor C_S is lost when the IGBT is turned on. The loss in the experimental circuit from this mechanism $P_{\rm snub}$ can be obtained as

$$\begin{aligned} P_{\rm snub} &= 8 C_S E^2 f \\ &= 8 \times 0.01\ \mu\text{F} \times (350\ \text{V})^2 \times 20\ \text{kHz} \\ &= 196\ \text{W}. \end{aligned} \tag{3}$$

As will be stated in Section V-B, the core loss in the transformer is estimated to be $P_{\rm core(tr)} = 20$ W. Therefore, the theoretical loss at $P_O = 0$ kW can be calculated as $P_{\rm snub} + P_{\rm core(tr)} = 216$ W, agreeing well to the experimentally observed value $P_{\rm loss} = 197$ W.

[2]In the experiment, isolated dc power sources for the gate drive circuits were obtained from the single-phase 100-V utility outlet via small-rated 50-Hz transformers and diode rectifiers. When $P_O = 10$ kW, the loss of the gate drive circuit for the eight IGBTs was 8.9 W. The loss corresponds only to 2.7% of the overall loss of the main circuit $P_{\rm loss} = 335$ W. Therefore, this paper discards the gate-drive circuit loss from the overall loss.

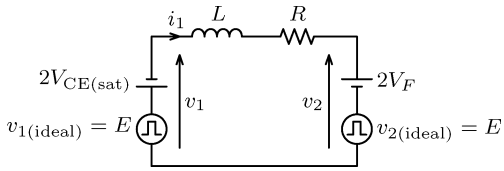

Fig. 13. Equivalent circuit of Fig. 6 where the winding resistance R of the transformer and the inductors, and the voltage drop across the power devices are taken into account.

V. Loss Analysis

A. Conducing Loss in the IGBTs

From the di_1/dt values in Figs. 9 and 10, one can estimate the voltage drop $2(V_{\mathrm{CE(sat)}} + V_F)$ across the power devices (two IGBTs and two diodes) at $P_O = 10$ kW. In Fig. 10, $di_1/dt = 30.4\ \mathrm{A}/\mu\mathrm{s}$ when $v_1 = E$ and $v_2 = -E$ so that the following equation exists:

$$L\frac{di_1}{dt} = 2E - Ri_1. \tag{4}$$

The second term in the above equation is negligible because it is obviously small compared to the first one (= 700 V). The inductance L can be calculated to be $L = 23.0\ \mu$H from the above equation. The following loss analysis uses not the value $L = 22.6\ \mu$H that appeared in Section IV-A but the value $L = 23.0\ \mu$H obtained here.

In Fig. 9, when $v_1 = v_2 = E$, the experimental circuit in Fig. 6 can be expressed by the equivalent circuit in Fig. 13. Note that Fig. 13 takes into account the winding resistance of the transformer and the inductors, and the voltage drop across the power devices. The voltages $v_{1(\mathrm{ideal})}$ and $v_{2(\mathrm{ideal})}$ would correspond to v_1 and v_2 if the power devices were ideal. In Fig. 9, $di_1/dt = -0.293\ \mathrm{A}/\mu\mathrm{s}$. Thus, the voltage drop across the power devices can be calculated as

$$2\left(V_{\mathrm{CE(sat)}} + V_F\right) = -L\frac{di_1}{dt} - Ri_1 = 5.9\ \mathrm{V}. \tag{5}$$

If i_1 in the above equation is approximated to be its average value of the absolute value, $\langle|i_1|\rangle$, the conducting loss P_{cond} in the power devices can be estimated to be

$$P_{\mathrm{cond}} = 2\left(V_{\mathrm{CE(sat)}} + V_F\right) \cdot \langle|i_1|\rangle = 189\ \mathrm{W}. \tag{6}$$

B. Losses in the Transformer and the Auxiliary Inductors

Table III summarizes the characteristics and losses of the transformer and each of the two identical auxiliary inductors at P_O =10 kW. The maximum flux density in the transformer core $B_{\mathrm{max(tr)}}$ can be calculated to be 0.86 T because the core effective cross-sectional area $A_e = 300\ \mathrm{mm}^2$, turn number (17 turns), the voltage $E = 350$ V, and the switching frequency $f = 20$ kHz have been already known. The maximum flux density in the auxiliary inductor $B_{\mathrm{max(ind)}}$ was obtained to be 0.174 T by using the rms value I_1 of the current i_1, 32.6 A. From the datasheets, the core losses can be estimated. The transformer core loss $P_{\mathrm{core(tr)}}$ was 20 W in Table III, the inductor core loss $P_{\mathrm{core(ind)}}$ was 9.0 W (4.5 W each).[3]

TABLE III
Characteristics and the Loss of the Transformer and the Inductors at the Rated Power of 10 kW

Parameter	Transformer	Inductor
Core Material	Finemet FT-3M	Ferrite PC44
Effective Cross Section	300 mm^2	328 mm^2
Effective Volume	60.7 cm^3	37.2 cm^3
Turn Number	17 : 17	6
Maximum Flux Density	0.86 T	0.17 T
Winding Resistance	17 mΩ	4.5 mΩ
Core Loss P_{core}	20 W	4.5 W
Copper Loss P_{copp}	18 W	4.8 W

The core losses were calculated based on the datasheets.

Two inductors were used in the experimental circuit.

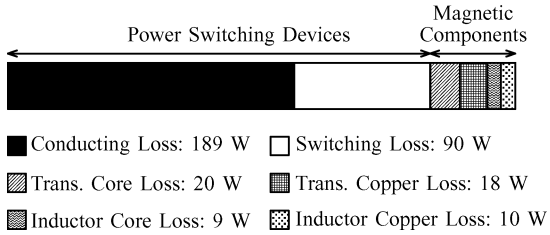

Fig. 14. Loss analysis in the experimental circuit.

The transformer winding resistance $R_{\mathrm{trans}} = 17\ \mathrm{m}\Omega$ and the rms current $I_1 = 32.6$ A produced the copper loss of $P_{\mathrm{cond(tr)}} = 17\ \mathrm{m}\Omega \times (32.6\ \mathrm{A})^2 = 18$ W in the transformer. Similarly, the inductor copper loss was $P_{\mathrm{cond(ind)}} = 4.5\ \mathrm{m}\Omega \times (32.6\ \mathrm{A})^2 \times 2$ inductors $= 9.6$ W.

C. Loss Analysis Results

Fig. 14 summarizes the loss analysis results. The switching loss P_{sw} in the figure was obtained by subtracting the power device conducting loss and the transformer and inductor losses from the overall loss $P_{\mathrm{loss}} = 335$ W. Although the "switching loss P_{sw}" in Fig. 14 may contain other losses than the real switching loss, the most dominant component in P_{sw} is the switching loss. Note that the snubber capacitor C_S theoretically does not contribute to the switching loss P_{sw} because each IGBT is operated in ZVS manner at 10 kW. The power loss produced by an equivalent series resistance existing in C_S is included in P_{sw}, but it may be negligible.

In Fig. 14, the loss in the power devices is 279 W and most dominant in the overall loss of 335 W. Therefore, significant loss reduction can be expected if the Si IGBTs are to be replaced by SiC power devices.

[3]The flux density in the transformer core becomes triangular because the rectangular voltages are applied to the transformer. On the other hand, trapezoidal current flows in the auxiliary inductors so that the flux densities in the auxiliary inductor cores also become trapezoidal. For the sake of simplicity, this paper deals only with the loss caused by the 20 kHz fundamental sinusoidal flux density.

TABLE IV
TRENDS IN THE BIDIRECTIONAL ISOLATED DC-DC CONVERTER

Year	1991	2005 (This work)	2015?
Switching Devices	First-Generation Si-IGBT	Latest Trench-Gate Si-IGBT	SiC-MOSFET/JFET
Core Material	Ferrite	Finemet^{TM†}	New Magnetic Material?
Efficiency (Loss)	around 91% (9%)*	97% (3%)	over 99% (1%)

* This value was estimated by the authors of this paper because the authors of [10] and [11] had made no description of efficiency.

† Nano-crystalline soft-magnetic material manufactured by Hitachi Metals

VI. POSSIBILITY OF LOSS REDUCTION BY SiC POWER DEVICES

A. Trends in SiC Power Devices

The breakdown field of SiC is ten times as high as that of Si so that high-voltage, low-loss, and high-speed unipolar devices can be realized. For example, while the specific on-state resistance in a 1.2-kV MOSFET drift region is theoretically limited to higher than 135 mΩcm^2 on Si, the use of SiC can reduce the theoretical limit to 0.248 mΩcm^2 [1]. In SiC–MOSFETs, the channel resistance is dominant because of low channel mobility. Thus, SiC–JFETs are also studied because their channel mobility is the same as that in the drift region [5]–[7].

Chang *et al.* have built a three-phase voltage-source inverter using SiC–JFETs (600 V, 25 A, 2.94 mΩcm^2)[4] and SiC-SBDs [5], and has reported that the on-state voltage across the JFET had been 38 m$\Omega \times$ 20 A $=$ 0.76 V. This value, 0.76 V, was less than the half of the voltage drop across the Si-IGBT used in this paper. Note that the SiC-JFETs in [5] were normally-on devices. Tone et al. have developed a normally-off SiC-JFET having a blocking voltage as high as 1,726 V and specific on-state resistance as low as 3.6 mΩcm^2 at 300 A/cm^2 [6]. Lai *et al.* have built single-phase and three-phase inverters using 500-V SiC–JFETs and have pointed out the synchronous rectification capability of the SiC–JFETs [7].

Arai and Yoshida have compared conducting and switching losses between 600-V Si–IGBTs and SiC–MOSFETs, and they have predicted both losses can be reduced to one-tenth [1]. SiC-MOSFETs, however, had suffered from relatively high channel resistance because high temperature (over 1,600 °C) annealing process had deteriorated the carrier mobility on the SiC–SiO_2 surface after acceptor ion implantation to create the p-well. Thus, new technologies to increase the channel mobility, as well as to reduce the channel resistance, have been invented to fabricate the following novel SiC-MOSFETs. In December 2004, Mitsubishi Electric reported that they had developed a 1.2-kV, 12.9-mΩcm^2 SiC-MOSFET, using epitaxial growth to create the p-well. At the same time, Rohm announced that a 1-kV, 7.15-mΩcm^2 SiC-MOSFET based on a improved process to create the gate oxide. In March 2005, the National Institute of Advanced Industrial Science and Technology of Japan (AIST) reported a 1.1-kV, 4.3-mΩcm^2 SiC–MOSFET [9]. The AIST SiC–MOSFET used also epitaxial growth to create the p-well. The conducting loss can be reduced to about one-fifth, compared to the 1.2-kV Si–IGBTs when the 1.1-kV SiC–MOSFETs and the 1.2-kV Si–IGBTs have the same current density as 100 A/cm^2.

[4]Parallel connection of four 0.02-cm^2 chips realizes the 25-A current rating.

B. Prediction of Conversion Efficiency With Use of SiC-MOSFETs and SiC-SBDs

Replacing Si–IGBTs with SiC–MOSFETs in Fig. 6 can reduce the conducting loss to a half to one-fifth. Using SiC–SBD can significantly reduce the switching loss because both the switching devices and the diodes are unipolar devices.

In the dc–dc converter that operates in rectification mode (Converter 2 in Fig. 6), the ac current flows mainly in two diodes. So far, the 1.2-kV SiC–SBDs from Infineon Technologies produces a forward voltage drop ranging from 1.5 to 2.1 V, which is much higher than the on-state voltage drop produced by the 1.2-kV SiC–MOSFET. However, synchronous rectification technique can be realized when using SiC-MOSFETs.

From the above-mentioned discussion, this paper assumes that the conducting loss $P_{\rm cond}$ can be reduced to one-fifth, and the switching loss $P_{\rm sw}$ can be reduced to one-tenth. As a result, the overall loss in the dc–dc converter at the rated power of 10 kW would be reduced from 335 W to 104 W, and so the efficiency of the dc–dc converter would reach $\eta = 99\%$.

Table IV summarizes trends in efficiency improvement and loss reduction of the dc–dc converter shown in Fig. 3(a). The dc–dc converter designed, constructed, and tested in this paper has reached the overall efficiency as high as 97%. As a result, the loss was reduced to one-third (from 9% to 3%) between 1991 and 2005. When SiC-MOSFETs/JFETs are available in the near future, the loss may be reduced to one-third again (3% to 1%).

In the 3.3-kV motor drive system in Fig. 5, the switching frequency of each cascaded PWM converter is 1 kHz so that the switching loss is small enough to be neglected, compared to that in the dc–dc converter with an overall efficiency of 99%. Therefore, the efficiency of each cascaded PWM converter may reach 99.5%. Thus, the overall efficiency of the 3.3-kV motor drive system is expected to reach $99.5\% \times 99\% \times 99.5\% = 98\%$ in 2015.

VII. CONCLUSION

This paper has described a technical issue in state-of-the-art medium-voltage power conversion systems, and has presented the next-generation 6.6-kV/3.3-kV power conversion systems intended to use SiC power devices. The proposed systems are characterized by providing galvanic isolation using the bidirectional isolated dc–dc converter to significantly reduce the size and weight of the system. In addition, this paper has designed

and built a bidirectional isolated dc–dc converter rated at 350 V, 10 kW, and 20 kHz as the core circuit of a 3.3-kV, 270-kW motor drive system. The results of loss analysis has revealed that using SiC power devices would realize the dc–dc converter with an efficiency of 99%, and the 3.3-kV, 270-kW motor drive system with an efficiency of 98%. This loss evaluation would encourage power electronics researchers and engineers to proceed with further research on this topology. Cost reduction and reliability improvement are the key to put these power conversion systems into practical use. These issues remain as the next phases of research.

REFERENCES

[1] K. Arai and S. Yoshida, *Fundamentals and Applications of SiC Devices*. Tokyo, Japan: Ohmsha, 2003.

[2] M. Kawai and C. Horikiri, "The invisible strength of power control semiconductors," (in Japanese) *Nikkei Electron.*, no. 893, pp. 79–97, 2005.

[3] J. A. Cooper, Jr. and A. Agarwal, "SiC power-switching devices—the second electronics revolution?," *Proc. IEEE*, vol. 90, no. 6, pp. 956–968, Jun. 2002.

[4] P. Friedrichs and R. Rupp, "Silicon carbide power devices—current developments and potential applications," in *Proc. Eur. Conf. Power Electron. Appl. (EPE)*, 2005, pp. 1–11.

[5] H.-R. Chang, E. Hanna, and A. V. Radun, "Development and demonstration of silicon carbide (SiC) motor drive inverter modules," in *Proc. IEEE Power Electron. Spec. Conf. (PESC)*, 2003, vol. 1, pp. 211–216.

[6] K. Tone, J. H. Zhao, L. Fursin, P. Alexandrov, and M. Weiner, "4H-SiC normally-off vertical junction field-effect transistor with high current density," *IEEE Electron Device Lett.*, vol. 24, no. 7, pp. 463–465, Jul. 2003.

[7] J.-S. Lai, H. Yu, J. Zhang, P. Alexandrov, Y. Li, J. H. Zhao, K. Sheng, and A. Hefner, "Characterization of normally-off SiC vertical JFET devices and inverter circuits," in *Proc. IEEE IAS Annu. Meeting*, Oct. 2005, vol. 1, pp. 404–409.

[8] G. Majumdar, "Future of power semiconductors," in *Proc. IEEE Power Electron. Spec. Conf. (PESC)*, 2004, vol. 1, pp. 10–15.

[9] S. Harada, M. Kato, M. Okamoto, T. Yatsuo, K. Fukuda, and K. Arai, "4.3 mΩcm^2, 1100 V normally-off IEMOSFET on SiC," in *Proc. Joint Tech. Meeting Electron Devices Semicond. Power Conv.* (in Japanese), 2005, pp. 27–31.

[10] R. W. De Doncker, D. M. Divan, and M. H. Kheraluwala, "A three-phase soft-switched high-power density dc–dc converter for high-power applications," *IEEE Trans. Ind. Appl.*, vol. 27, no. 1, pp. 63–73, Jan./Feb. 1991.

[11] M. H. Kheraluwala, R. W. Gascoigne, and D. M. Divan, "Performance characterization of a high-power dual active bridge dc-to-dc converter," *IEEE Trans. Ind. Appl.*, vol. 28, no. 6, pp. 1294–1301, Nov./Dec. 1992.

[12] G. Spiazzi, S. Buso, M. Citron, M. Corradim, and R. Pierobon, "Performance evaluation of a schottky SiC power diode in a boost PFC application," *IEEE Trans. Power Electron.*, vol. 18, no. 6, pp. 1249–1253, Nov. 2003.

[13] N. Okada, "Control of loop distribution network and result," in *Proc. IEEJ Tech. Meeting Power Syst. Eng.* (in Japanese), 2000, pp. 2–12.

[14] P. W. Hammond, "A new approach to enhance power quality for medium voltage ac drives," *IEEE Trans. Ind. Appl.*, vol. 33, no. 1, pp. 202–208, Jan./Feb. 1997.

[15] M. Pavlovsky, S. W. H. de Haan, and J. A. Ferreira, "Concept of 50 kW dc–dc converter based on ZVS, quasi-ZCS topology and integrated thermal and electromagnetic design," in *Proc. Eur. ConfePower Electron. Appl. (EPE)*, 2005, pp. 1–9.

[16] H. Stemmler, "State of the art and future trends in high power electronics," in *Proc. Int. Power Electron. Conf. (IPEC)*, Tokyo, Japan, 2000, vol. 1, pp. 4–14.

[17] N. Schibli and A. Rufer, "Single-phase and three-phase multilevel converters for traction systems 50 Hz/16 2/3 Hz," in *Proc. Eur. Conf. Power Electron. Appl. (EPE)*, 1997, vol. 4, pp. 210–215.

[18] G. Kratz and H. Strasser, "Antriebskonzept füur zukünftige elektrische Triebfahrzeuge," *Elektr. Bahnen*, vol. 96, pp. 333–337, 1998.

[19] L. Heinemann, "An actively cooled high power, high frequency transformer with high insulation capability," in *Proc. IEEE Appl. Power Electron. Conf. Expo (APEC)*, 2002, vol. 1, pp. 352–357.

Shigenori Inoue (S'02) was born in Fujimi, Japan, on January 29, 1979. He received the B.S. and M.S. degrees from Tokyo Metropolitan University, Tokyo, Japan, in 2002 and 2004, respectively, and is currently pursuing the Ph.D degree at the Tokyo Institute of Technology.

He is currently a Research Fellow with the Japan Society for the Promotion of Science (JSPS). His research interests include medium-voltage power conversion systems, bidirectional isolated dc–dc converters, and active power filters.

Hirofumi Akagi (M'87–SM'94–F'96) was born in Okayama, Japan, in 1951. He received the B.S. degree from the Nagoya Institute of Technology, Nagoya, Japan, in 1974, and the M.S. and Ph.D. degrees from the Tokyo Institute of Technology, Tokyo, Japan, in 1976 and 1979, respectively, all in electrical engineering.

In 1979, he joined the Nagaoka University of Technology, Nagaoka, Japan, as an Assistant and then Associate Professor in the Department of Electrical Engineering. In 1987, he was a Visiting Scientist at the Massachusetts Institute of Technology (MIT), Cambridge, for ten months. From 1991 to 1999, he was a Professor in the Department of Electrical Engineering, Okayama University, Okayama, Japan. From March to August 1996, he was a Visiting Professor at the University of Wisconsin-Madison and then M.I.T. Since January 2000, he has been a Professor in the Department of Electrical Engineering, Tokyo Institute of Technology. He has published 68 IEEE TRANSACTIONS papers and two invited IEEE Proceedings papers. He has made presentations many times as a Keynote or Invited Speaker internationally. His research interests include power conversion systems, ac motor drives, high-frequency resonant-inverters for induction heating and corona discharge treatment processes, and utility applications of power electronics such as active filters for power conditioning, self-commutated BTB systems, and FACTS devices.

Dr. Akagi received two IEEE IAS TRANSACTIONS prize paper awards in 1991 and in 2004, two IEEE PELS TRANSACTIONS prize paper awards in 1999 and in 2003, nine IEEE IAS Committee prize paper awards, the IEEE William E. Newell Power Electronics Award in 2001, and the IEEE IAS Outstanding Achievement Award in 2004. He was elected as a Distinguished Lecturer of the IEEE Industry Applications and Power Electronics Societies for 1998–1999. He is currently President of the IEEE Power Electronics Society.